EARSeL Workshop on TOPOGRAPHY FROM SPACE
8-10 June 1994
Chalmers University of Technology, Göteborg, Sweden

USE OF C-BAND ARCS IN SPACEBORNE (ERS-1) AND AIRBORNE (TOPSAR) SAR MISSIONS

G. DE CAROLIS
GNCB - CNR, Bari, Italy
S. PONTE
Faculty of Engineering, Univ. of Naples "Federico II", Napoli, Italy
F. POSA
c/o Physics Dept., Polytechnic of Bari, Italy
V. SCHENA
Co.Ri.S.T.A., Consortium for Research on Advanced Remote Sensing Systems, Napoli, Italy

Use of C-band active radar calibrators in spaceborne and airborne SAR missions

G De Carolis
GNCB-CNR, Bari, Italy

S. Ponte
Faculty of Engineering, University of Naples "Federico II", Napoli, Italy

F Posa
Physics Dept., Polytechnic of Bari, Bari, Italy

V.D Schena
Consortium CO.RI.S.T.A., Napoli, Italy

ABSTRACT: This paper is addressed to the description and performance analysis of the C-band ARCs developed under a collaboration between the Consortium for Research on Advanced Remote Sensors (CO.RI.S.T.A., Naples, Italy) and the University of Bari (Bari, Italy). The main design considerations and the hardware performance of the active devices are presented. Furthermore, the laboratory measurements of radar cross-section (RCS) and propagation delay time are compared to the ones obtained from SAR data acquired during spaceborne (ERS-1) and airborne (AIRSAR-TOPSAR) campaigns. The radiometric calibration of the SAR images, performed with the intensity integration method, allowed us to recover the RCS of the ARCs within ±0.8 dB: the RCS values obtained from the calibrated images are in good agreement with the experimental measurements, within the laboratory calibration error (±0.6 dB).

1 INTRODUCTION

With respect to their passive counterpart, i. e. the trihedral corner reflectors (CR), Active Radar Calibrators (ARC) offer to the field of external calibration of synthetic-aperture radar (SAR) systems unique advantages such as design flexibility, reduced dimensions, relatively small sensitivity to positioning errors, large and adjustable radar cross-section (RCS). This paper deals with the C-band ARCs developed since 1991 by the consortium CO.RI.S.T.A. (Naples, Italy) and the University of Bari, Italy. Currently, three C-band ARCs are operational, and have been widely used during past external SAR calibration campaigns.

The main laboratory measurements performed to characterise the hardware performance are presented, together with the procedures aimed at the characterisation with respect to the variation of parameters critically related to the RCS. In addition, ARC responses collected from spaceborne (ERS-1, ESA) and airborne (AIRSAR-TOPSAR, NASA/JPL) SAR imagery are considered.

Results from laboratory analysis and calibrated SAR images provide a comprehensive understanding of the ARCs' performance, allowing one to gain insight into the use of active devices in ground calibration missions. Moreover, with a full characterisation of an ARC, the experimenters can exploit the great potentialities of such devices in different applications, such as the evaluation of the SAR's end-to-end system response function, cross- and co-polarised, the assessment of in-flight azimuth antenna patterns, the acquisition of amplitude and phase characteristics of multi-channel and multi-polarisation SARs.

2 DESCRIPTION OF THE ARC

Figure 1 shows a block diagram of the C-band ARC.

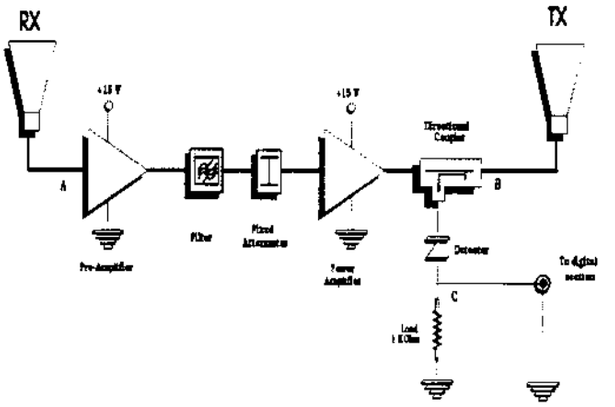

Figure 1. C-band ARC: block diagram of the RF section.

The active device basically consists of a receiving (RX) and a transmitting (TX) antenna coupled with a radio-frequency (RF) amplifier section. Signal detection circuitry has been designed with the aim of feeding a portion of the received power to a digital data acquisition section, capable of indicating with a

LED the duration of the illumination corresponding to the overpass of the microwave sensor. It is possible to store the received signal, digitally converted by an A/D section and routed to a parallel interface, by means of an acquisition card (Ground Receiver), in order to evaluate the azimuth antenna pattern.

The receiving horn antenna is connected to a preamplifier, built in hybrid technology and cascaded with a band-pass filter, centred on the desired frequency (5.3 GHz) and with a maximum available bandwidth of ≅400 MHz. The chosen bandwidth is a compromise between the need of filtering out spurious signals and noise, and the possibility of using the same ARC for future or different SAR systems. A second amplification stage is provided by a power amplifier connected after a fixed attenuator, which arranges the dynamic range of the received signal between the two stages. During the prototypal realisation, a variable attenuator was used to have a suitable range of RCS values, so as to avoid both saturation of the SAR impulse response function and positive feedback in the RF section.

The directional coupler spills a fraction of the input power (10 dB below the power amplifier output) to a detector diode, connected to ground by a 1-kΩ resistor which adjusts the sensitivity. The result of the detection is the envelope of the radar signal in a negative pulse train at the pulse repetition frequency (PRF). Finally, the signal is re-radiated to the passing-by sensor through a horn with the same characteristics of the receiving one.

In the following we summarise the main aspects and characteristics of the ARC.

1 packaging. Electronics and antennas are weatherproof and the structure is able to withstand normal winds without readjustment. Deployment and orientation are easily accomplished, and the adjusting/locking mechanisms are manual, independent for each antenna which can be oriented at 45°, 90° and ° with respect to the other. The device weighs about 20 kg.

2 power requirements. Lead-gel airtight batteries supply 12 V, 10 Ah, and an electronic power step-up DC-DC converter supplies 15 VDC to the RF section The power supply allows 10-hours full operation, with a current absorption of 650 mA. The external power source is easy to connect and replace, with circuitry to protect against wrong insertions.

3 amplifier section. A LED turns on when the ARC is receiving a power greater than or equal to the peak expected power. Both the preamplifier and the power amplifier have gain flatness of ±0.05 dB over the available bandwidth (Table 2), with noise figure of 3.6 dB at the centre frequency.

4 antennas. Both RX and TX antennas, labelled for easy identification, are C-band pyramidal horns with rectangular aperture (13.2x9.4 cm). The -3 dB beamwidths in the E and H-planes are 25° and 34°respectively, values which overcome orientation problems. To achieve good cross-coupling, the distance between the centre of symmetry of the two horns has been set to 62 cm. At 5.3 GHz the antennas have a bandwidth of 300 MHz. The peak gain declared by the manufacturer is 15 dB (Table 3), with typical sidelobe levels of -20 dB which reduce multipath effects and background noise. In addition to the orientation of the antennas with respect to the flight line, a different polarisation state is achieved by rotating each antenna about its boresight at 45° steps, with a system of hexagonal-head bolts on a frame structure. Echo-absorbing material surrounds the horns, in order to avoid resonance effects and to minimise re-radiation effects of the structure (Fig. 2).

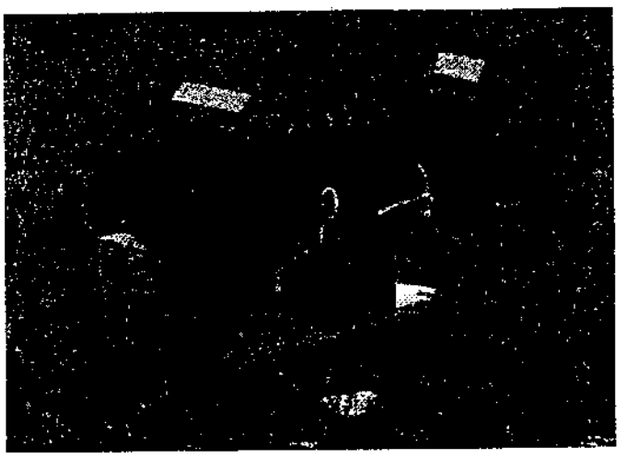

Figure 2. C-band ARC.

3 MEASUREMENTS AND VALIDATION

In order to obtain a full characterisation of the active device, the following measurements were carried out:

1. Output power as a function of the input power (i.e. transfer function of the device).
2. Gain over the frequency bandwidth.
3. Thermal characterisation.
4. Antenna characterisation.

3.1 Transfer function measurement

The measurement set-up for the evaluation of the RF gain of the ARC as a function of the input power is shown in Figure 3. A synthesised sweeper generator is connected to the input of the device under test (DUT) with a step attenuator whose output is set 30 dB below the input level. The RF output of the DUT (point B in the figure) is connected to a spectrum analyser. A digital multimeter was used for voltage measurements. During the measurements, the temperatures of the room and the device were monitored by a K-type probe (NiCr-NiAl thermocouple) and a digital multimeter acting as a thermometer. A chirp signal with 5.3 GHz carrier frequency and 600 MHz

bandwidth, produced by the signal generator, represented the input to the DUT.

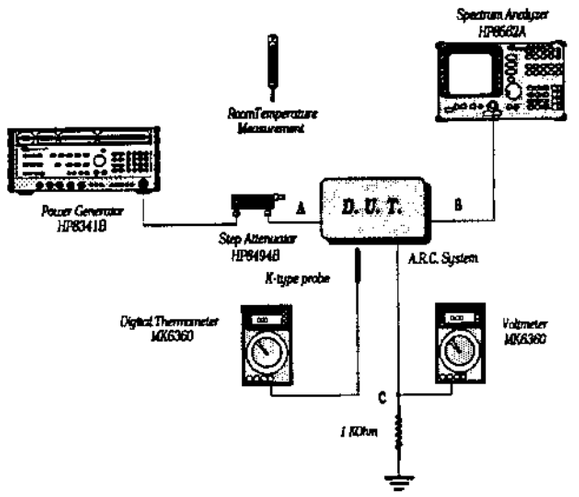

Figure 3. Experimental set-up for gain measurement.

The room temperature was constant (20.5 °C), whereas the device took 15 minutes to reach the temperature of 36.6 °C, which did not change during the measurement procedure. In Figure 4 the transfer function of the amplifier section is shown.

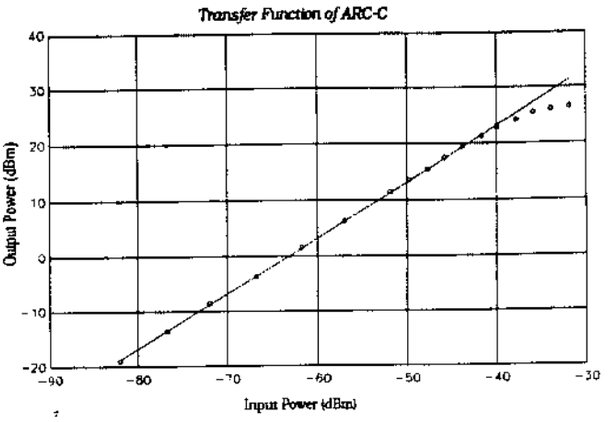

Figure 4. Measured transfer function of the C-band ARC.

The step attenuator allowed us to scan power levels from -82.00 dBm to -31.85 dBm using a high and constant value of the generated signal. In this way the signal -to-noise ratio is improved. However, given an input signal level, the effect of the noise was taken into account by averaging a set of measurements and considering the root mean square (rms) value. An error equal to ± 0.05 dB was found, but ± 0.5 dB was measured for the two lowest input values. Great stability on the output results was observed, so that we assumed an error of ≅0 dB. This behaviour is due to the so-called *ballast effect* introduced by the resistors compounding the device and the double stage of the ARC amplifier section (Figure 1) (Cheung and Owens 1981, Carlson 1992).

We used two custom amplifiers produced by JCA, a pre-amplifier (model JCA56-353) which includes into the package a band-pass filter centred on 5.3 GHz with a bandwidth of 300 MHz, and the JCA56-519 power amplifier. Both amplifiers are made in hybrid technology. Table 1 reports the factory technical characteristics. By means of Table 1 and the Friis' formula for cascaded amplification stages (Carlson 1992), the maximum value of the noise figure of the ARC amplifier was estimated as 2.5 dB.

Table 1. Technical data of the JCA amplifiers.

Device name	JCA56-353	JCA56-519
Frequency Range	5.1 to 5.5 GHz	5.0 to 5.6 GHz
Gain (dB)	27 (min.)	43 (min.)
Gain Flatness (dB)	±1.0 max.	±1.5 max.
Noise Figure (dB)	2.5 max.	4.5 max.
Power Output (dBm)	10 min. (-1dB)	25 min. (-1 dB)
Input VSWR	2:1 max.	2:1 max.
Output VSWR	2:1 max.	2:1 max.
DC Power	+15 V @ 150 mA	15 V @ 550 mA

The transfer function exhibits linearity between -95 dBm and about -40 dBm. In this range a linear least-square fit (Bevington and Robinson 1992) was performed to evaluate the line slope and intercept with their uncertainty values. Table 2 reports the numerical values of the parameters of the linear fitting. The value 2.262 assures that the true value of the sample is bounded within the given uncertainty with 97.5% probability (Capiluppi *et al.* 1978), whereas the rms errors on the slope (m) and on the intercept (n) are indicated with Δm and Δn, respectively.

Table 2. Parameters of the straight-line fitting.

	Theoretical formula	Numerical value [dBm]
Slope	$m \pm 2.262\Delta m$	1.005 ± 0.006
Intercept	$n \pm 2.262\Delta n$	-63.310 ± 0.078

Above the input value of -40 dBm, saturation of the amplifier section occurs. The 1-dB compression point, i.e. the input value where the amplifier's output power deviates from the extrapolated value by 1 dB, is located at -37.85 dBm. The absolute value of the intercept represents the mean gain of the amplifier section calculated after integration on the bandwidth. This value has been found to be 63.31 dB. The same measurements were carried out for the available three ARCs. In Table 3 the corresponding gains are reported, together with the standard deviations (the contribution from the antennas is not considered).

Table 3. C band ARC data.

Device	Gain [dB]	Standard deviation [dB]
ARC #1	60.55	±0.06
ARC #2	60.76	±0.08
ARC #3	63.31	±0.08

3.2 Gain over the frequency bandwidth

The measurement set-up used to characterise the amplifier section of the ARC with respect to the frequency is shown in Figure 5.

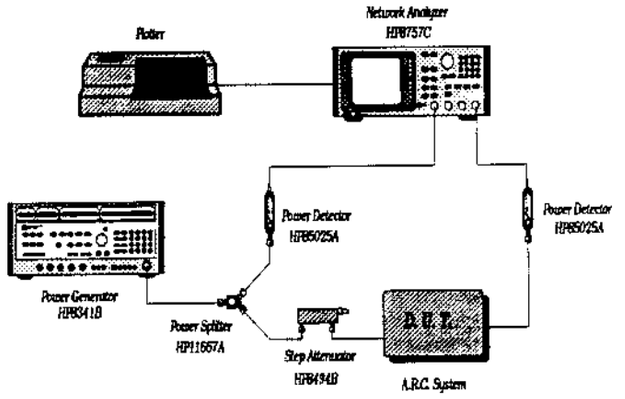

Figure 5. Measurement set-up for the frequency-domain analysis.

This kind of measurement allowed us to evaluate the performance of the filter and the overall gain flatness. The signal from the synthesised sweeper generator is divided by a power splitter. One of the outputs feeds the DUT and a power detector, and the other one enters another power detector. The outputs from the power detectors are sent to a scalar network analyser connected to a plotter. In Figure 6 the output diagram provided by the scalar network analyser is shown.

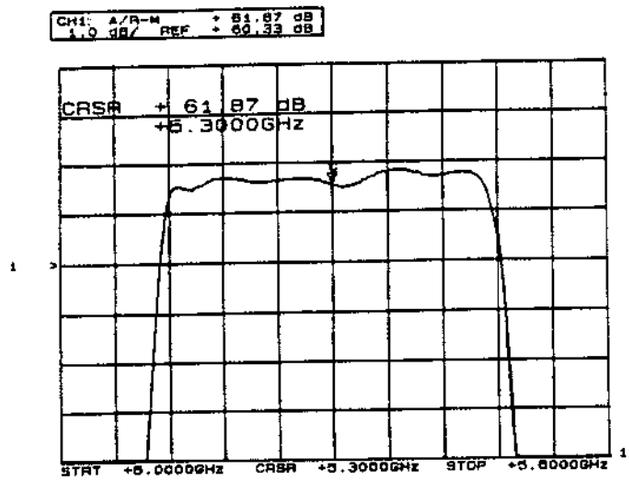

Figure 6. Plot of gain over frequency for the C-band ARC

The measured bandwidth of the filter was in good agreement with the nominal one. The gain flatness is about ± 0.2 dB, which is better than the values reported on the data sheet of the single components of the amplifier section (Table 1). This improvement can be again explained as a ballast effect.

3.3 Thermal characterisation

The purpose of thermal measurements was to evaluate changes of the ARC's RF gain with respect to variations of room temperature. The "thermal" assessment is very important for ARCs because they are expected to work in open-air sites at different temperature and humidity conditions during SAR campaigns.

The DUT was placed into a thermal room and the device input was connected to a synthesised CW generator (Model HP8671B) set up on a power level of -60 dBm, a typical value of the received power during *in situ* operation. The DUT output was connected to a spectrum analyser (Model TK2792), and the temperature was detected by a K-type probe, connected to a digital thermometer. The temperature was changed with 10 °C steps from - 5 °C to + 55 °C every 30 minutes, in order to get stabilised values. The uncertainty on the temperature measurements is about 0.5 °C. In this way a wide range of air conditions were simulated.

In Figure 6 the experimental RCS values as a function of the temperature and both the linear and fourth-order polynomial fittings are reported. The rms errors of the fit are also given. It can be noted that the rms values of the fits are quite similar.

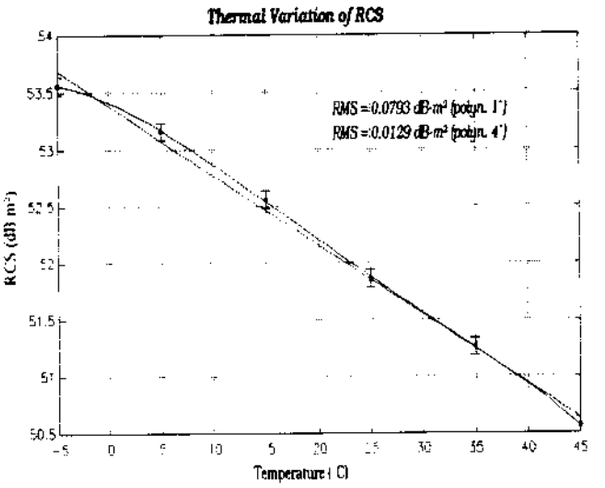

Figure 6. Comparison between 4-th order polynomial and linear fitting on the thermal data.

In order to evaluate the radar cross-section of the ARCs, the following formula was used (Brunfeldt and Ulaby 1984).

$$\sigma_{ARC} = \frac{\lambda^2}{4\pi} G_{ARC} G_{Ant}^2 \qquad (3.1)$$

where σ_{ARC} is the calculated RCS, λ is the wavelength at the centre frequency (0.05656 m), G_{ARC} is the measured gain of the RF section with mismatch and insertion losses, and G_{Ant}^2 is the product of the

receiving and transmitting antenna gains. The linear fit allowed us to calculate $\Delta RCS/\Delta T$, i.e. the change rate of the RCS with respect to the temperature, given by the slope of the straight line. We found:

$$\frac{\Delta RCS}{\Delta T} \cong 0.06 \text{ dBm}^2 \text{ °C}^{-1} \qquad (3.2)$$

which indicates good thermal stability.

3.4 Antennas characterisation

The two pyramidal horn antennas are built with a short waveguide containing a radiator cut on $\lambda/4$, resonating at 5.3 GHz. The radiator can be connected to an external coaxial cable by means of a SMA connector. In Table 4 the factory technical data are reported.

Table 4. Antenna factory data.

Specification	Value
Frequency [GHz]	5.3
Bandwidth [MHz]	300
Gain at -3 dB [dB]	15 (min.)
Beamwidth at boresight [deg]	15
Return loss [dB]	17 (min.)
Cross polarisation isolation [dB]	32 (min.)
Sidelobe level* [dB]	-17 (min.), -20 (min.)

*For horizontal (H) and vertical (V) polarisation.

For fine characterisation of the antennas, some measurements were made into an anechoic chamber: gain, in order to evaluate return loss (RL), voltage standing wave ratio (VSWR), mismatch loss (ML) and decoupling with respect to polarisation.

The well-known standard-gain antenna method has been used for gain measurement. The measurement set-up consisted of a standard antenna (NARDA Model 643) with known gain G_{st}, connected by a fixed attenuator (-3 dB) to a CW generator (Model HP8671B) working at 5.3 GHz. The antenna under test was connected by a fixed attenuator to a spectrum analyser and placed at a distance R from the standard antenna. The unknown gain, G_{Test}, was evaluated as (Laverghetta 1981):

$$G_{Test} = \frac{4\pi R^2}{\lambda} \frac{P_r}{P_t} \frac{1}{G_{st}} \qquad (3.3)$$

where P_r and P_t are respectively the received and transmitted power. The measured gain ranges from 15.50 dB to 16.06 dB for all C-band antennas. The other measurements were made by a double-output directional coupler connected to the antennas under test and to a CW generator. Table 5 reports the measured values: VSWR is the average voltage standing wave ratio. As a final remark, it is worth saying that the measurement accuracy was 0.6 dB, including the error contributions of the gain-measuring system (up to 0.3 dB), instabilities of the antenna gain over temperature (0.1 dB), thermal noise and multipath errors (of the order of 0.2 dB).

Table 5. Antenna parameters: measured values.

Description	Value	
Gain [dB]	15.5 - 16.06	
Return loss [dB]	20.00	
Mismatch loss [dB]	0.05	
VSWR	1.22	
Decoupling*	$V_1 V_2 > 60$ dB	$H_1 H_2 > 54$ dB
	$V_1 H_2 > 82$ dB	$H_1 V_2 > 82$ dB

*Pedices indicate TX antenna (1) and RX antenna (2).

4 USE OF C-BAND ARCs IN SAR EXTERNAL CALIBRATION CAMPAIGNS

The validation of the laboratory measurements and the assessment of correct ARC performance during ground calibration campaigns were performed by analysing C-band calibrated data, gathered from different SAR systems. The main goals of the calibration experiments, namely image quality assessment and radiometric calibration, have been accomplished by deploying on both the test-sites two ARCs and several trihedral corner reflectors with different RCS, used as reference targets. In the following, after a brief description of the strategy adopted for radiometric calibration of SAR images, the main results of our analysis on radar data will be presented.

4.1 Radiometric calibration

The images were calibrated by using the intensity integration method (Gray *et al.* 1990), insensitive to focusing errors and processor coherence. It is based on the estimates of E_{gp}, the energy associated to a reference reflector deployed on the ground and imaged in the data set, E_{gu}, the background clutter energy, and the image noise power, whereas the accuracy of the estimates derives from the standard deviation of E_{gp}, evaluated on different reference targets. The average backscattering coefficient in correspondence of each point target, $\langle\sigma^0\rangle$, is given by:

$$\langle\sigma^0\rangle = \sigma_{ref} \frac{E_{gu}}{A_u E_{gp}} \sin\vartheta_u \qquad (4.1)$$

where A_u is the area swept by the slant range and azimuth spacings, and viewed under a look angle of ϑ_u. The reference RCS, σ_{ref}, and the estimates of the energy term E_{gp} were derived from the CRs deployed on the test site, as it will be described later. The amplitude-calibrated image, proportional to $\langle\sigma^0\rangle$, was used to recover the RCS of the ARCs, by

evaluating the product $E_{gp}A_p$ on the area A_p, containing the response of the active calibrator. The accuracy of the method, which depends on the speckle autocovariance function and on the background clutter (Ulander 1991) has been found to be of the order of 0.7 dB for the TOPSAR data set, and 0.8 dB for the ERS-1 images.

4.2 MAC-Europe 1991 Campaign (TOPSAR)

The multisensor airborne campaign (MAC) organised in Europe in 1991 gave to our research group the possibility of setting up a calibration experiment on the Matera test-site, gathering data from the NASA DC-8 Airborne SAR (AIRSAR), augmented with a pair of C-band antennas displaced across-track (Topographic Synthetic-Aperture Radar, TOPSAR, Zebker *et al.* 1992). Three C-band ARCs and 26 trihedral CRs were deployed on homogeneous background, and interferometric data were acquired during five passes (Alberti *et al.* 1994). One of the images of the interferometric couple, processed by CO.RI.S.T.A., is shown in Figure 7: the brightest ARC, No. 1, is visible on the centre of the image, just above the upper diagonal line of CRs with different leg lengths (the four brightest CRs, on the left, have 180 cm leg length).

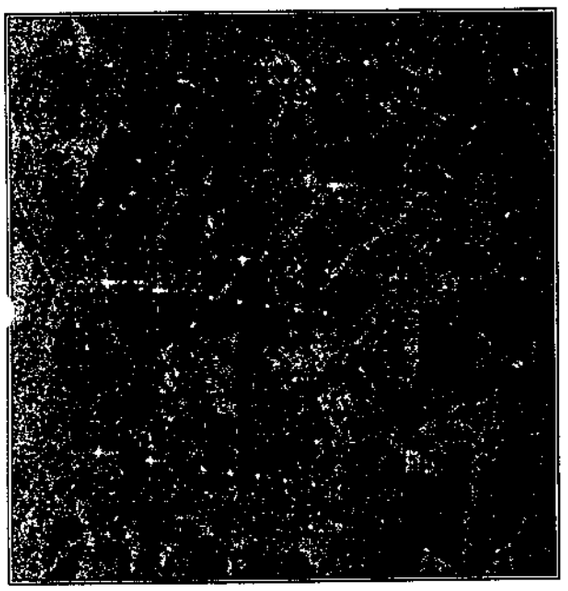

Figure 7. TOPSAR image of the test-site (June 25, 1991 pass)

A measurement of the propagation delay time of the ARC was carried out and compared with the laboratory data. The calibrated images allowed us to recover the ARCs' RCS and delay times in good agreement with the anechoic chamber tests, as reported in Table 6

Table 6. Comparison between laboratory measurements and estimates from TOPSAR data (ARC No. 1).

Parameter	Laboratory	SAR image
RCS [dBm²]	43.28±0.6	43.6±0.8
Delay time [ns]	30±0.5	44±11

The uncertainty on the delay time, measured on the SAR images, is due to the ratio between the velocity of light and the slant range spacing, and is ±11 ns. The values are referred to ARC No. 1: similar results were obtained from ARC No. 3, whereas ARC No. 2 did not work during the overpass of the sensor, due to hardware malfunctioning.

4.3 Experiment I-7, 1991-92 (ERS-1)

In the framework of the Experiment I-7, ERS-1 SAR data were acquired during the October 23, 1991 night pass over the Salento Peninsula and June 21 and July 7, 1992 day passes over Matera (Southern Italy). Two ARCs and various corner reflectors were deployed on both sites. The analysed data sets are extracted from Single-Look Complex (SLC) products provided by the SAR Verification Mode Processor (VMP) installed at the Earthnet Program Office of the European Space Agency (ESA-ESRIN, Frascati, Italy) and from Precision Image (PRI) products processed at the Italian Processing and Archiving Facility (I-PAF), Matera. A detailed report on the first results of this experiment can be found in Caffório *et al.* 1993.

The two PRI images provided by the I-PAF processor were calibrated by using the ESA transponder responses of the Oct. 13, 1991 Flevoland acquisition, according to ESA's criteria. The energy terms were estimated on a region of 4-times interpolated 51x51 pixels, bye evaluating E_{gp} on a subset of 31x31 pixel centred on the mainlobe peak, and the background clutter from the remaining side pixels. The computed calibration constant was applied to the data sets, in order to estimate the RCS of the active devices deployed on the test- sites The calibration results are summarised in Table 7, where σ_{exp} is the expected RCS. The differences from the expected (laboratory) values are mainly due to the lack of thermal stabilisation, a problem that was solved later in 1993. Moreover, a temperature variation of about 25 °C was recorded, due to different seasons and acquisition times. The mean look angle was 22 degrees.

Table 7. Radiometric analysis of the PRI 1991/92 products.

Date	Oct. 23, 1991		July 7, 1992	
ARC #	1	2	1	2
σ_{exp} [dBm²]	54.80	56.80	52.00	52.00
σ [dBm²]	56.25	59.51	55.45	54.70

The thermal stabilisation of the ARC, performed via a compensation look-up table in the prototypal version, was improved in late 1993 with cooling fins. During the first months of 1994, two "revised" C-band ARCs were deployed on the salt-works of Margherita di Savoia (Puglia, Southern Italy), a test-site with very low clutter echo return, due to the presence of large evaporite ponds (average depth: 80 ÷100 cm) surrounding the ARCs' locations. The images analysed (PRI product, delivered by the I-PAF, in slant range format, with 3 azimuth looks) refer to two night passes of the satellite, namely, January 28th, 1994 and February 3rd, 1994 (Fig. 8).

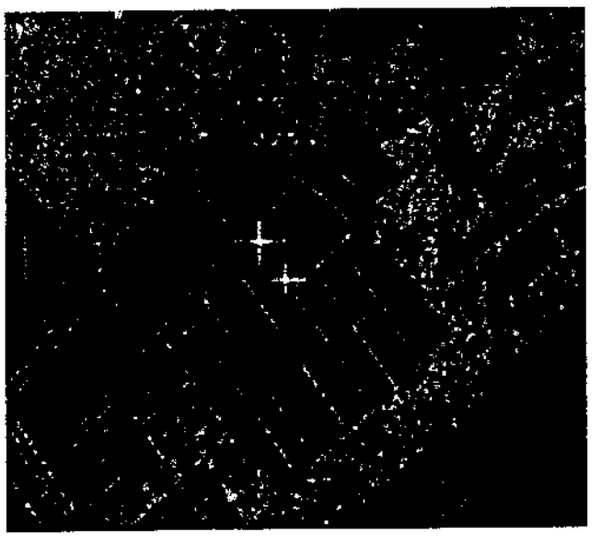

Figure 8. PRI image of the ARCs (Feb. 3, 1994 pass).

The mean temperature during the acquisitions was 9 °C, and the wind speed was 40 knots during the first pass (Jan. 28th), about 10 knots during the second pass. The active devices were deployed on the embankments in central position, at a distance of about 200 m, to minimise coupling effects. The results of the radiometric calibration, performed with the intensity integration method, are shown on Table 8, whereas a point target analysis confirmed the good geometric and radiometric processor quality, with the resolutions, Integrated Sidelobe Ratio (ISLR) and Peak Sidelobe Ratio (PSLR) well within the ESA specifications. The spatial resolution is 25x25 m². The accuracy on the radiometric calibration is rather good (about 0.5 dB), even if a small number of estimates of E_{gp} were available, because of the low background clutter from the ponds.

Table 8. Radiometric analysis on 1994 PRI products.

Date	Jan. 28, 1994		Feb. 3, 1994	
ARC #	1	2	1	2
σ_{nom} [dBm²]	52.6	52.6	52.6	52.6
σ° [dBm²]	51.5	53.0	53.5	51.7

5 CONCLUSIONS AND FURTHER WORK

This paper has dealt with the development and use of C-band ARCs in SAR external calibration campaign. Laboratory measurements and results from radiometrically calibrated SAR images have shown good stability and performance of the active devices, which are the natural substitutes of conventional CRs, overcoming the stability and size problems of passive devices with the same radar cross-section. In addition, unique characteristics could be exploited, such as the possibility of tuning the propagation delay time with suitable devices (for example, microwave fibre-optic delay lines). This characteristic could be useful for calibration applications: forcing the point target response in a more convenient location on the image, the energy terms of Eq. (4.1) could be estimated very accurately by minimisation of the backscattering from pixels surrounding the ARC response. Moreover, a tunable delay time means a controlled phase shift on the complex echo return, and this could be useful for interferometrical applications, allowing one the estimation of processor-induced phase errors.

On the basis of the experience gained by our research group during the last few years, and starting from the satisfactory results obtained from laboratory and on-the-spot tests, future developments on our active devices could be summarised in the following points:

1. Development of a ground acquisition section, in order to monitor the in-flight azimuth antenna pattern by detecting the strength of the signal received during the synthetic-aperture formation time. Successful laboratory tests on a digital section interfaced to a PC strongly encouraged us to test the ARC by attempting to record the SIR-C/X-SAR azimuth pattern, last April. As soon as the official data from this sensor are available, we will verify and validate our results. The possibility of collecting the range antenna pattern is obviously related to the number of ARCs necessary to sample the range swath: at the moment, such a sampling is far from adequate, due to the little number of ARCs developed.

2. Accurate laboratory measurement of the phase stability of the ARC. By characterising the phase shift induced by the active device up to fractions of radians, it should be possible to trace our ARCs as a reliable phase reference. Work is currently underway on the implementation of such measurements.

3. Development of a set of multi-frequency ARCs. With suitable X-band and L-band ARCs it will be possible to calibrate data from new operational multi-frequency SAR systems (such as SIR-C/X-SAR), extracting information on the electromagnetic behaviour of the imaged area at different wavelengths, and analysing the antenna patterns with appropriate ground receiver sections.

ACKNOWLEDGEMENTS

This work is being carried out under an Italian Space Agency (ASI) contract. We would also like to thank Eng. L. Garamone, responsible of the Microwave Laboratory of the ASI Spatial Geodesy Center (Matera, Italy).

REFERENCES

Alberti, G., Vetrella, S., Moccia, A., Ponte, S. 1994. Analysis and results of the TOPSAR experiments in Southern Italy. *EARSeL Advances on Remote Sensing*, Vol. III, No. 1, in press.

Bevington, P. R., Robinson, D. K. 1992. *Data reduction and error analysis for the physical sciences.* New York: McGraw-Hill.

Brunfeldt, D. R., Ulaby, F. T. 1984. Active Reflector for Radar Calibration. *IEEE Trans. on Geoscience and Remote Sensing*, GE-22: 165-169.

Calabrio, C., De Carolis, G., Mattia, F., Moccia, A., Monte, S., Posa, F., Schena, V. D., Sergi, R., Smacchia, P., Sozzi, V., Vetrella, S. 1993. Preliminary results of the experiment I-7. *Proc. 1st ERS-1 Symposium, Cannes 4-6 Nov. 1992*. ESA SP-359: 161-166.

Capiluppi, A., Postpischl, D., Randi, P. 1978. *Introduzione alla elaborazione dei dati sperimentali.* Roma: CLUEB.

Carlson, A. B. 1992. *Communication systems.* Singapore: McGraw-Hill.

Cheung, W. S., Owens, R. 1981. *Microwaves made simple*. Norwood: Artech House.

Gray, A. L., Vachon, P. W., Livingstone, C. E., Lukowski, T. I. 1990. Synthetic aperture radar calibration using reference reflectors. *IEEE Trans. on Geosc. Rem. Sens.*, GE-28: 374-383.

Laverghetta, T. S. 1981. *Handbook of microwave testing.* Norwood: Artech House.

Ulander, L. M. H. 1991. Accuracy of using point targets for SAR calibration. *IEEE Trans. Aerosp. Electronic Syst.*, 27: 139.148.

Zebker, H. A., Madsen, S. N., Martin, J., Wheeler, K. B., Miller, T., Lou, Y., Alberti, G., Vetrella, S., Cucci, A. 1992. The TOPSAR interferometric radar topographic mapping instrument. *IEEE Trans. on Geosc. Rem. Sens.*, 30: 933-940.